PROTON IRRADIATION OF CENTAUR, KUIPER BELT, AND OORT CLOUD OBJECTS AT PLASMA TO COSMIC RAY ENERGY

JOHN F. COOPER
Raytheon Technical Services Company LLC, SSDOO Project, NASA Goddard Space Flight Center, Greenbelt, MD, U.S.A.
(E-mail: jfcooper@pop600.gsfc.nasa.gov)

ERIC R. CHRISTIAN
Office of Space Science, NASA Headquarters, Washington, D.C., U.S.A.

JOHN D. RICHARDSON[1] and CHI WANG[1,2]
[1] *Center for Space Research, Massachusetts Institute of Technology, Cambridge, MA, U.S.A.;*
[2] *Laboratory for Space Weather, Chinese Academy of Sciences, Beijing, China*

Abstract. Times for accumulation of chemically significant dosages on icy surfaces of Centaur, Kuiper Belt, and Oort Cloud objects from plasma and energetic ions depend on irradiation position within or outside the heliosphere. Principal irradiation components include solar wind plasma ions, pickup ions from solar UV ionization of interstellar neutral gas, energetic ions accelerated by solar and interplanetary shocks, including the putative solar wind termination shock, and galactic cosmic ray ions from the Local Interstellar Medium (LISM). We present model flux spectra derived from spacecraft data and models for eV to GeV protons at 40 AU, a termination shock position at 85 AU, and in the LISM. Times in years to accumulate dosages ∼100 eV per molecule are computed from the spectra as functions of sensible surface depth less than one centimeter at unit density. The collisional resurfacing model of Luu and Jewitt is reconsidered in the context of depth-dependent dosage rates from plasma, suprathermal, and higher energy protons, and global exposure, by micrometeoroid dust grain impacts, of moderately irradiated red material below a thin crust of heavily irradiated neutral material. This material should be more visible on dynamically 'cold' objects in the ∼40 AU region.

1. Introduction

The 'bubble' of solar wind plasma and frozen-in magnetic fields expanding out from the solar corona, within a few radii of the Sun, to boundaries with the local interstellar gas and plasma near about 100 AU is called the heliosphere. Dependent on points of origin at the Sun, and on time phase during the eleven year cycle of solar activity, the solar wind plasma expands radially outward at speeds of 300–800 km/s. Neutral atoms flowing into the heliosphere from the Very Local Interstellar Medium (VLISM) can be ionized by solar UV, and by charge exchange with solar wind ions, then picked up by magnetic fields in the outward plasma flow. Due to inverse-square fall-off of solar wind ion density with distance from the Sun, these interstellar pickup ions increasingly contribute to the plasma pressure and become the dominant component beyond the orbit of Saturn (Burlaga et al.,

Earth, Moon and Planets **92:** 261–277, 2003.

1996; Whang et al., 1996). Further out near 90–100 AU (Stone, 2001; Stone and Cummings, 2001; Whang and Burlaga, 2002) the outflowing plasma is expected to encounter the solar wind termination shock where flow speeds abruptly transition to sub-sonic values ∼100 km/s. The shock position is dependent in part on the plasma and neutral gas density in the Local Interstellar Medium (LISM) and could move into the giant planet region, or even nearer to the Earth's orbit, if the Sun passed through a region of much higher LISM density (Zank and Frisch, 1999; Frisch, 2000). Further out at 120 AU or more should be the heliopause, the contact boundary between the diverted solar wind plasma flows and the in-flowing interstellar plasma. The intervening region between the termination shock and the heliopause is called the heliosheath. In this latter region the previously radial flow of the solar wind is diverted into a direction downstream from the ∼26 km/s flow of the interstellar gas to form a huge teardrop-shaped structure called the heliotail which extends hundreds to perhaps thousands of AU from the Sun into the VLISM.

Within the heliosphere the interplanetary environment of solar wind plasma, solar (SEP) and interplanetary energetic particles, and galactic cosmic rays (GCR) has long been surveyed *in-situ* beyond Neptune's orbit at 30 AU, since 1983 and 1990 by the Pioneer 10 and 11 spacecraft, and since 1987 and 1989 by Voyager 1 and 2. Of these, the Pioneers are no longer transmitting data and the Voyagers are now respectively at 89 and 71 AU, far beyond the 48 AU semi-major axis (a) cutoff of the Classical KBO population but within the range of aphelia $48 < Q < 10^3$ AU for known Centaurs (perihelia at $5 < q < 35$ AU) and Scattered KBOs ($q > 35$ AU). Voyager 1 is expected to cross the termination shock, later followed by Voyager 2, within the next several years and possibly to exit the heliosphere across the heliopause within its remaining ∼17 + years of operational lifetime. Both spacecraft will have been silent for millennia before reaching the Oort Cloud region at 10^4 to 10^5 AU. Within the next quarter century NASA may launch an interstellar probe (e.g., Mewaldt et al., 2001a) moving outward at 10 AU/year with the ultimate goal of surveying the VLISM environment out to several hundred AU. Until then, the next mission to the outer solar system is planned to be New Horizons (Stern and Spencer, 2003), which will fly by the Pluto/Charon system in 2015 and thereafter attempt several flybys of accessible KBOs. Enroute to Pluto this mission may attempt at least one Centaur flyby after swinging by Jupiter in 2007.

The principal goal of this paper is to utilize plasma and energetic ions data from heliospheric spacecraft measurements to model the heliocentric radial variation in ion irradiation fluxes potentially affecting the visible surface chemistry of the KBOs, highly eccentric Centaurs with $Q > 40$ AU, and Oort Cloud comets. Near the orbit of Earth we rely on time-averaged measurements (e.g., Mewaldt et al., 2001b) from the Advanced Composition Explorer (ACE) spacecraft located in L1 halo orbit 10^6 km from the Earth along the Earth–Sun line, while comparable data are provided by the two Voyager spacecraft in the outer heliosphere. Between ACE and the Voyagers, and beyond radial positions of the latter out into the VLISM, we must rely on available models for radial and temporal variations of the plasma

and energetic ion flux spectra. The data we are using extend from 1 eV only up to several keV for plasma ions, but above 0.1 MeV/nucleon for energetic ions, so we must also extrapolate in energy with upper and lower flux limits across the intermediate, so-called suprathermal range. The plasma model we are now using only applies to protons, pending future work in progress on other species, so the results here are only for protons across the full energy range from 1 eV to 10 GeV.

Over a wide range of depths the proton component tends to dominate irradiation effects of electronic ionization in the affected bodies, but there are effects of surface sputtering, implantation, and elastic nuclear energy loss for which heavy ions become more important at very shallow depths $\lesssim 1$ μm. We do compute both the electronic and elastic nuclear components of proton energy loss but do not include secondary particle and photon production from inelastic nuclear scattering. Since the inelastic collision lengths for primary ions incident on solid icy material are tens to hundreds of centimeters, assuming unity density, our energy deposition model is restricted to depths less than one centimeter. At meter depths, interactions of secondary charged particles (p, α, $e^{\pm}$, $\pi^{\pm}$, $\mu^{\pm}$), neutrons, and gamma rays are dominant. At much greater depths the natural radioactive decay of some heavy nuclei in the icy surfaces and denser cores of cometary bodies becomes the main energy source for radiolytic chemistry (e.g., Draganić et al., 1987; Johnson, 1990).

2. Heliospheric and LISM Proton Flux Model

2.1. Plasma distributions

A very new development from our earlier work (Cooper et al., 1998, 2001a) is the inclusion of proton energy distributions from a model described below for plasma protons at eV to keV energy from the solar wind plasma and from pickup of photo-ionized inter-stellar hydrogen in the ~400 km/s flow as measured to date by Voyager 2 out to 71 AU. The Voyager 1 plasma spectrometer has not been fully operational since 1980, so plasma distributions and moments (speed, density, temperature, pressure) are available only from Voyager 2. Figure 1 shows the density and temperature profiles from the model for solar wind protons, pickup protons, and the interstellar neutral hydrogen. Only a small percentage of thermal energy from pickup ions is needed to produce the observed non-adiabatic radial profile in temperature for the solar wind protons.

For the heliospheric plasma ion distributions at 40 and 85 AU we use the three-fluid, one-dimensional solar wind model of Wang and Richardson (2001, 2003). The model includes solar wind protons, pickup protons, and electrons, each assumed to have Maxwellian distributions, relaxed over time from more anisotropic initial distributions as interstellar hydrogen atoms are charge-exchanged to form the pickup ions. The interstellar neutral distributions are computed self-consistently using a hydrodynamic approach. The solar wind protons and interstellar neutrals are coupled by charge exchange interactions. An energy partition

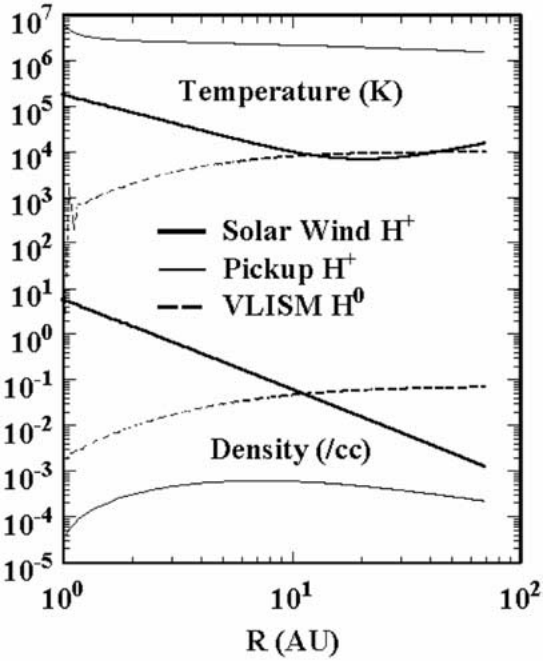

Figure 1. Heliocentric radial profiles for temperature (K) and density of solar wind and pickup plasma ions, and of interstellar neutral hydrogen, from the multi-fluid, spherically symmetric MHD model of Wang and Richardson (2001, 2003). Not shown is the solar wind proton speed, which slows slightly in response to pickup ion pressure.

ratio is used to represent the division of energy provided by the pickup process between solar wind and pickup protons. The initial solar wind conditions at the inner boundary at 1 AU are radial outward speed $V = 441$ km/s, solar wind proton density $N = 7.0$/cc and temperature $T = 9.8 \times 10^4$ K, and interplanetary magnetic field $= 7.0 \times 10^{-5}$ Gauss. The interstellar hydrogen atoms at the solar wind termination shock are taken to have speed 20 km/s and temperature 1×10^4 K, while H^0 density, and the energy partition ratio for ions, are varied to give good fits to radial speed and temperature profiles measured by the operational plasma spectrometer on Voyager 2. Good fits are obtained for a neutral density of 0.09/cc and a partition ratio of 0.05, which means that five percent of the total energy from the pickup process goes into solar wind protons. For the LISM plasma ions, which are not included in the Wang and Richardson model, we compute convecting maxwellian (Vasyliunas, 1971) distributions for the LISM parameters $T \sim 7000$ K, $u \sim 26$ km/s, and $N \sim 0.1$/cc of interstellar protons as derived from Wood and Linsky (1997).

In the moving frame of a convecting plasma the speeds of ions with mass m are specified by an isotropic maxwellian distribution for density N and temperature T. In the inertial frame along the axis of convection there is a convective maxwellian

distribution for ions moving along this axis. In Equation (1) below the unidirectional number flux j, given as a function of ion kinetic energy E, is defined for ions moving at inertial speed v and convected with the entire thermal distribution at speed u, in the positive direction along such an axis. Units are cgs for m, N, v, and the Boltzman constant k, in Kelvin (K) for T, and in MeV for E. The factor $f = 1.602 \times 10^{-6}$ converts to MeV from cgs energy units of ergs.

$$j(E) = \frac{fN}{(2\pi mkT)^{1/2}} e^{\frac{-m}{2kT}(v(E)-u)^2} \quad \text{(protons/cm}^2\text{-s-MeV)}. \tag{1}$$

Modeling of plasma ion irradiation for semi-spherical icy bodies requires averaging over directions of ion incidence along and perpendicular to the axis of solar wind radial flow. As a first approximation for simplicity of computation we assume that there are separate populations of ions moving unidirectionally towards a spherical surface from six directions. These are parallel and anti-parallel to positive directions along three orthogonal axes X_i centered at the irradiated object: X_1 for radial flow outward from the Sun in the Ecliptic, X_2 in direction of prograde orbital motion around the Sun, and X_3 in the northward direction from the Ecliptic. The global average directional flux (ions/cm^2-s-sr-MeV) at energy E onto this surface is given simply by $J(E) = [j_+(E) + j_-(E) + j_\perp(E)/4\pi$ where the first two terms in brackets are for parallel and antiparallel flows along X_1, while the third is the sum of all flows into the surface on the two other perpendicular axes. The $\frac{1}{4}$ factor arises from unidirectional flow from any direction onto a sphere of arbitrary radius r, cross-sectional area πr^2, and total surface area $4\pi r^2$, while the $1/\pi$ factor converts from unidirectional flow units to directional flux for the case of isotropic flow onto a locally flat surface. Slow rotation of irradiated bodies eliminates asymmetric irradiation effects due to radial solar wind flow, so it is reasonable to define an isotropic directional flux J_0 equivalent to globally averaged surface fluxes J, and this is used to show flux spectra of the plasma ions later in the paper. For radiation dosage computations versus depth the local current flow into an irradiated spherical surface is πJ_0.

The relative amplitudes of the three major flow components (j_+, j_-, and $j_\perp$) are determined by the directionality and thermal widths of the three different types of proton distributions (solar wind H^+, pickup H^+, LISM H^+) at the given temperatures for each type. Radial flow of the solar wind and pickup ions is of course a major factor for j_+ and j_-, while isotropic temperature in the moving frame is dominant for $j_\perp$. In Figure 2A the high convection speed $u \sim 400$ km/s and low temperature $T \sim 9 \times 10^3$ K of the solar wind H^+ distribution at 40 AU results in a very narrow energy distribution around the convection speed energy $E \sim 1$ keV, and a completely separate $j_\perp$ component at low energy due only to the thermal distribution. For higher temperature $T \sim 2 \times 10^6$ K of the pickup H^+ distributions at 40 AU (Figure 2B), and low convection speed $u \sim 26$ km/s of the LISM H^+ distributions (Figure 2C), there are substantial j_- components, and the three components overlap in energy. The proton distributions at 85 AU near the

assumed termination shock position are qualitatively similar to those at 40 AU, the principal change being a decline in solar wind proton density. Note from Figure 1 that charge exchange equalizes temperatures of solar wind H^+ and interstellar H^0 in the 10 to 70 AU range.

2.2. Cosmic ray proton distributions

For the present work we define 'cosmic ray' protons as being those with energies above 0.1 MeV from sources within and outside the heliosphere. Sources include solar energetic particle (SEP) events, acceleration by interplanetary shocks and the solar wind termination shock, and inward diffusion through the heliosheath of galactic cosmic rays thought mostly to be accelerated by interstellar shocks from supernova explosions. Protons and heavier ions accelerated at the termination shock, after pickup from photo-ionization of interstellar gas neutrals, are called anomalous cosmic rays (ACR). The seed population of energetic protons for the cosmic ray source extends down a few keV, below which lie the plasma protons discussed above. Up to 0.1 MeV we designate constituents of this seed population as the suprathermal ions.

One of our co-authors, E. R. Christian, has worked as part of the Mewaldt et al. (2001b) collaboration to produce a long-term fluence model for selected heavier ions (He, O, Fe) from data acquired near 1 AU by the Advanced Composition Explorer (ACE) spacecraft. This model extended from plasma energies > 0.3 keV/nucleon up to 300 MeV/nucleon for fluences integrated over about three years from October 1997 to June 2000, a period of rising solar activity from minimum to maximum conditions. For the 1-AU baseline of the present work we have used the ACE data above 0.1 MeV/nucleon from three instruments: the Ultra-Low Energy Isotope Spectrometer (ULEIS), the Solar Isotope Spectrometer (SIS), and the Cosmic Ray Isotope (CRIS) Spectrometer. One limitation of ACE composition data is that only the $Z > 1$ ions are measured to avoid instrument saturation by high proton intensities, particularly during large SEP events. However, since Mewaldt et al. (2001b) found that flux spectra of different ions showed similar shapes of energy distribution, i.e., power-law at keV/nucleon to MeV/nucleon energies, we have inferred the 1-AU proton fluence spectrum from standard abundance ratios for H/He and the ACE He fluence spectra from ULEIS, SIS, and CRIS.

During the same time interval covered by Mewaldt et al. (2001b) the Cosmic Ray (CRS) experiments on the Voyager 1 and 2 spacecraft respectively acquired spectral flux data at 68–78 AU and 53–61 AU for protons and heavier ions above 0.1 MeV/nucleon. These data were of course not acquired in-situ for the < 50 AU orbits of the Classical KBOs and less eccentric Centaurs. We instead use GCR flux spectra computed at 40 and 85 AU, shown in Figure 3, from a one-dimensional cosmic ray transport model with parameter fits to peak fluxes during conditions of minimum solar activity in the mid-1990s at ACE and the two Voyager spacecraft, which gives maximum limits for radiation effects of GCR ions. GCR source spec-

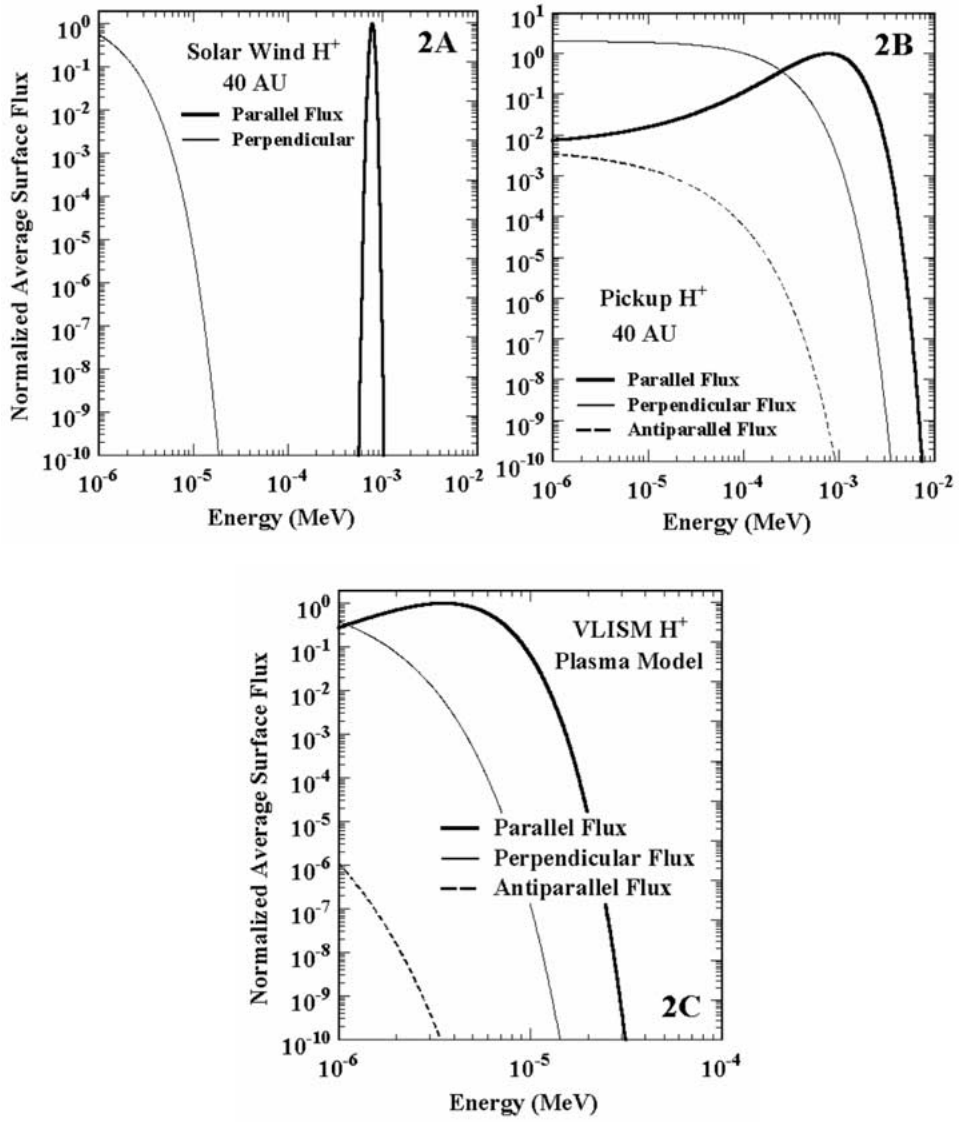

Figure 2. Normalized components at 40 AU of the solar wind (Panel 2A) and pickup (Panel 2B) proton flux spectra incident onto a spherical body from directions parallel, antiparallel, and perpendicular to radial outward flow from the Sun. There is no antiparallel component for (2A) due to relatively low temperature and high convection speed. The same components are shown in Panel 2C for the VLISM proton spectra.

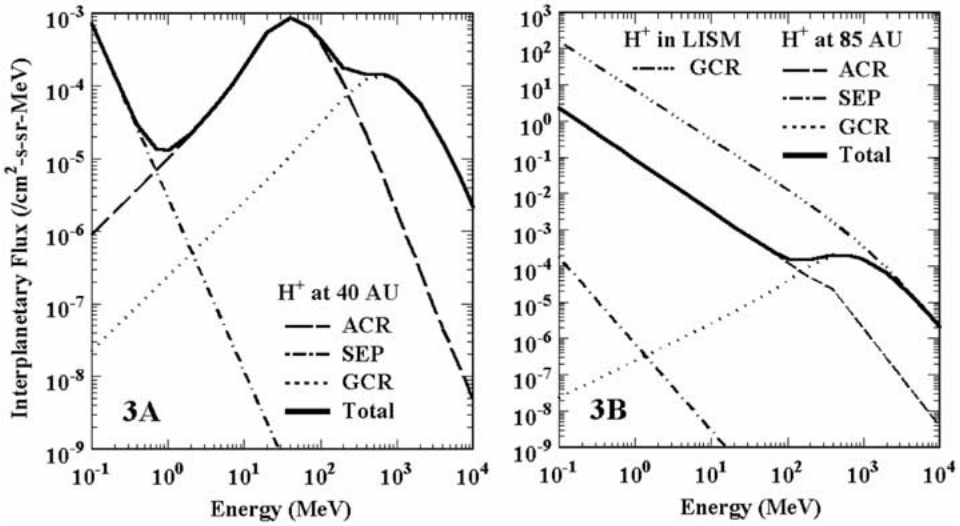

Figure 3. These two panels show components of a heliospheric proton model compiled by E. R. Christian and J. F. Cooper for 40 AU (left panel), an earlier assumed position of the solar wind termination position at 85 AU (right panel), and the LISM (right panel). The total H^+ flux is shown also separated out into three constituents: solar energetic particles (SEP), anomalous cosmic ray (ACR) component of cosmic rays accelerated at the termination shock, and galactic cosmic rays (GCR) from sources outside the heliosphere.

tra in the LISM are defined here from work of Webber and Potgieter (1989) for power-law flux spectra (vs. E) of the form $\sim p^{-2.75}$ in terms of proton momentum $p(E)$ from models of interstellar shock acceleration. The SEP proton spectra in Figure 3 were estimated from ULEIS and SIS fits for time-averaged flux spectra at ACE by means of an inverse-square power law with solar distance. Aside from any further acceleration that may occur by interaction with interplanetary shocks during SEP ion propagation outward from 1 AU, this gives a reasonable upper limit on SEP proton fluxes in the outer solar system. However, adiabatic energy loss in the expanding solar wind likely produces even steeper fall-off in SEP fluxes.

Near solar minimum the ACR ions, including protons, are dominant components of radiation dosage outward from ~40 AU to the outer heliosphere, while these ions largely disappear at solar maximum. There is a 22-year cycle in the polarity of the solar dipole magnetic field, which is frozen into the solar wind plasma within several radii of the Sun and thereby carried outward into the heliosphere. Due to sign-dependent transport effects, the ACR ions accelerated at the termination shock have larger fluxes, and more positive radial gradients, at 40 to 85 AU near the Ecliptic when the solar dipole moment is directed southward ($qA < 0$ polarity) than when it is northward ($qA > 0$ polarity). At the 85-AU termination shock for our model Figure 3 shows the ACR flux spectra determined for this location from Voyager CRS data (Cummings and Stone, 1996, 1998; Stone et al., 1996) for mid-1994. These ACR spectra are for the $qA > 0$ solar magnetic polarity and

are intermediate in intensity between very low ACR fluxes at solar maximum and the six-times higher fluxes at the $qA < 0$ solar minimum in 1987. Plots of the total H^+ fluxes at the termination shock and in the LISM from this model were earlier published by Cooper et al. (2001a), but the flux spectra reported there for the termination shock were plotted incorrectly and are actually several orders of magnitude lower for protons. A corrected version of the termination shock spectra was also recently reported in Strazzulla et al. (2003). At 40 AU the modulated ACR spectra are computed from the 1-D transport model for diffusion in from the source flux at 85 AU with model parameters determined from fits to the peak fluxes at the Voyagers.

2.3. Composite proton flux spectra

In Figure 4 we show for each region the composite of proton flux spectra at plasma and cosmic ray energies, along with low and high limits on suprathermal fluxes in between these energy regimes. The low suprathermal limit is defined by the power-law extension of the cosmic ray spectrum to an intersection with the high-energy side of the plasma distribution. The high limit is drawn from the cosmic ray endpoint to join with the convective peak of the plasma distribution. From visual comparison of the three panels in Figure 4 it is evident that proton flux levels increase over a wide range of energy less than 100 MeV at the three selected spatial regions from 40 AU to the LISM. Radial gradients, corrected for latitudinal differences, in ~10 to 20 MeV/nucleon ACR intensity between Voyager 1 and 2 vary from zero at $qA > 0$ solar minima to less than ten percent/AU for $qA < 0$ minima, although there were some negative (< 10%/AU) and larger positive (< 20%/AU) excursions during solar maximum in 1990–1991 (Cummings and Stone, 1998). Generally positive radial gradients are consistent with the primary source of the ACR ions being at the termination shock. At GeV energies the GCR protons are only weakly affected by solar modulation, so there is little difference from the LISM into the heliosphere.

On the Voyagers the suprathermal range is covered above tens of keV by the Low Energy Charged Particle (LECP) experiments on each spacecraft, but these instruments do not distinquish between protons and heavier ions, and the measured fluxes are highly variable. In the future we will consider long-term averages of the LECP fluxes with the reasonable assumption of count rate dominance by protons, but the present limits allow initial estimates to be made on radiation dosage contributions of the three energy regimes: plasma, suprathermal, and cosmic ray. Time averaging over solar cycles will also be needed at plasma and cosmic ray energies, and the ACR component actually needs averaging over 22-year solar magnetic cycles, i.e., over the 25-year span of Voyager measurements from 1 AU to the outer heliosphere. In the LISM there are presently no direct measurements but we can hope to acquire these at suprathermal to cosmic ray energies by ~2020 if at

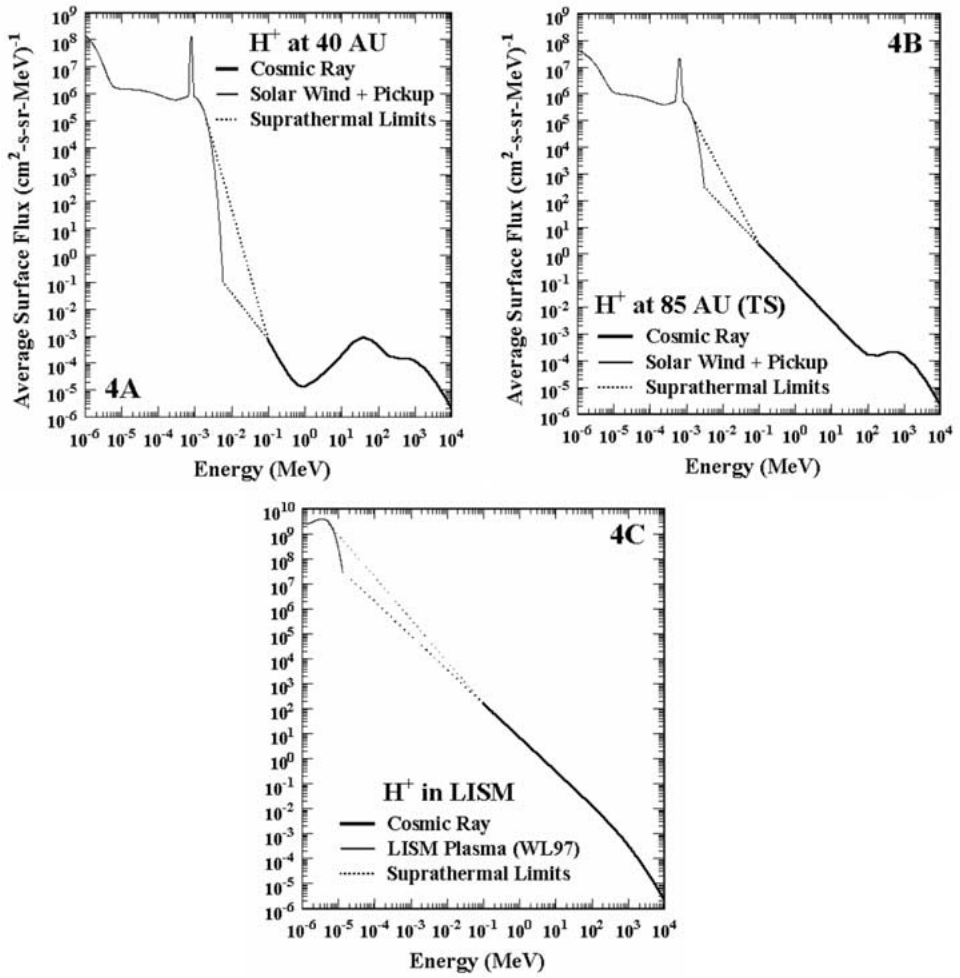

Figure 4. Composite spectrum models of average surface flux for thermal, extrapolated suprathermal, and cosmic ray proton spectra at (A) 40 AU, (B) an assumed solar wind termination shock position at 85 AU, and (C) outside the Heliosphere in the LISM. WL97 refers to Wood and Linsky (1997).

least a still operational Voyager 1 crosses the heliopause into the local interstellar environment by that date.

3. Radiation Dosage

For protons the primary radiation dosage process is deposition of energy within the volume of material as a function of depth. This deposition occurs either by electronic ionization of target atoms or by direct collisions with nuclei within the atoms. Nuclear collisions are purely elastic, as for billiard balls, up to some threshold energy for inelastic collisions, which can also excite or break up the

struck nucleus with increasing effect at higher energies. The present work is limited to dosages from electronic ionization and elastic collisions, and the differential energy loss rates in MeV/cm for water are maximal at different energies, 100 eV for nuclear collisions versus 100 keV for electronic ionization. Thus the plasma protons mostly lose energy by nuclear collisions while ionization becomes dominant for suprathermal and cosmic ray protons. Inelastic collisions producing secondary particles become important at proton energies above a few hundred MeV, where electronic energy loss approaches minimum levels. However, energy loss in a given layer is dominated by protons stopping in that layer, and vertically incident protons above 30 MeV penetrate beyond the top 1-cm layer of interest here. Since space irradiation acts over a range of surface incidence angles from the vertical, higher energy protons incident at large angles also contribute in this top layer.

The three panels of Figure 5 show times in years to accumulate chemically significant dosages in the standard unit of 100 eV per 16-amu for water ice from the corresponding flux spectra in each panel of Figure 4. Curves for the electronic ionization and elastic nuclear collision components of proton energy loss, and the results using the upper and lower limits on suprathermal spectra in the 1–100 keV range, are shown separately. The procedures used here to compute volume dosage rates as functions of surface depth are the same as described by Cooper et al. (2001b) for magnetospheric ion irradiation of Galilean moons in Jupiter's magnetosphere, except that the lowest ion energy has been extended down to 1 eV to accommodate the plasma model data. Differential energy loss and range data for protons incident on water ice were computed, as in Cooper et al. (2001b), from the Stopping and Range of Ions in Matter (SRIM) code of Ziegler et al. (1985) at http://www.SRIM.org/.

Exclusion of secondary electromagnetic and nuclear interactions results in overestimates of dosage times due to high energy protons above a few hundred MeV from the GCR source. Near 1 AU the output from the CREME-96 cosmic-ray dosage model of Tylka et al. (1997) indicates a limiting time scale $\sim 2 \times 10^9$ years from this component, as reported earlier by Cooper et al. (2001a). Since the GCR protons are decreasingly affected by solar modulation as secondary processes become dominant at the higher energies, $\sim 10^9$ years is the limiting time throughout and beyond the heliosphere due to secondary effects.

The time-vs-depth curves show important limits and trends related to distribution of proton flux in energy and solar distance. Time scales of 10^4 to 10^6 years computed for depths less than 0.01 μm are probably unrealistically short, since surfaces are continually (1) gardened by interplanetary and interstellar dust impacts (Yamamoto and Mukai, 1998; Landgraf et al., 2002) and (2) sputtered (Johnson, 1990) by protons and heavier ions at eV to MeV energies. Irradiation products at such depths are thereby either eroded away into space or mixed to deeper levels and correspondingly lower concentrations. At 40 AU the times for chemically effective dosages fall sharply below the 10^9-year GCR secondary interaction limit only at depths less than 0.1 μm and with little difference between the electronic and nuc-

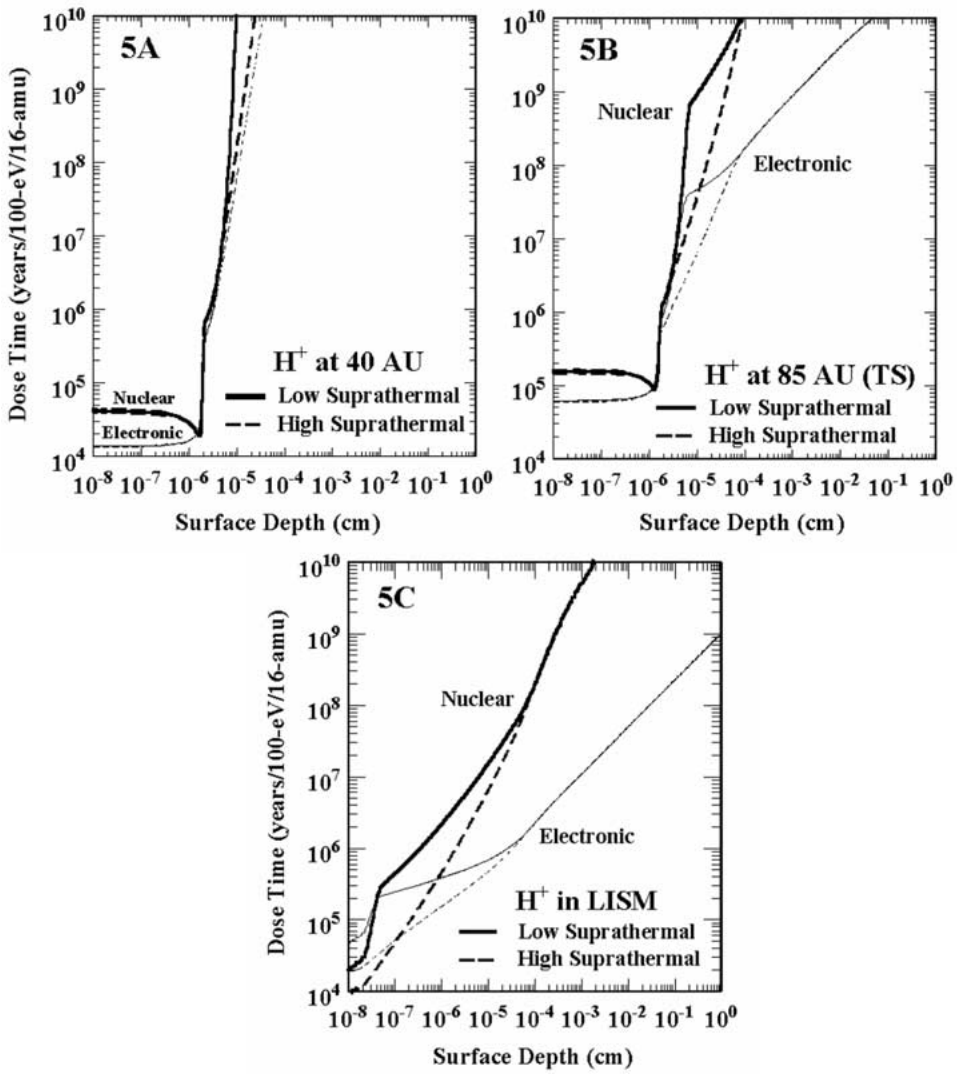

Figure 5. Times in years for accumulation of radiolytically significant dosages of 100 eV per 16-amu in proton-irradiated material (e.g., Johnson, 1990; Strazzulla and Johnson, 1991) versus surface depth for water ice at unit density. Solid and dashed curves in each panel, 5A–5C, are for irradiation from composite proton spectra in the corresponding panels of Figure 4 at low and high suprathermal limits. Two sets of curves are shown for proton energy loss from electronic ionization (thin curves) and elastic nuclear collisions (thick curves). Secondary interaction processes such as electron bremsstrahlung production of gamma rays and inelastic nuclear collision production of nucleons (p, n, α), pions, and muons are not included.

lear dosages, such that the sensible layer to 1-cm depth is minimally processed. For the 85-AU termination shock location the times at 0.1-μm depth drop to 10^7 to 10^8 years, while in the LISM the electronic time scale even at 1 cm is below the 10^9-year limit. Flux and dosage rates increase by orders of magnitude in this depth range from 40 AU out into the LISM. From 40 AU to the termination shock this trend reflects the positive radial intensity gradient for ACR protons diffusing inward from the shock acceleration source.

Future spacecraft measurements will show if energetic proton fluxes fall off beyond the shock at points within the heliosheath and beyond the heliopause in the VLISM less than 10^3 AU from the Sun. Present models suggest maximal dosage rates in the LISM. Thus Oort Cloud comets, and possibly Scattered KBOs with aphelia near the heliosheath and VLISM, are maximally irradiated, while Classical KBOs near 40 AU are minimally irradiated. Radial intensity gradients $\lesssim +10\%$/AU of ACR ions might account for spatial variations in color within this latter population, e.g., redder objects with increasing perihelia in the $32 < q < 45$ AU range as reported by Doressoundiram et al. (2002) and at this conference by Doressoundiram (2003).

For radiation chemistry models, we cannot assume, however, that all irradiated objects start with the same primordial composition. Objects accreted at different distances and temperatures in the early solar nebula may have very different surface composition ranging from pure water ice to refractory crusts with high abundances of organic molecules. In these proceedings, Moore et al. (2003) and Moroz et al. (2003) discuss laboratory measurements of the different products that arise from irradiation of various such materials. Initially bright mixtures of H_2O, CO, N_2, and CH_4 can evolve under irradiation to more complex (in some cases, redder) molecules (Moore et al., 2003) but eventually become spectrally neutral (Moroz et al., 2003) as organics are carbonized. Reddening is thus a possible intermediate effect, but not necessarily the final state after billions of years of irradiation.

It has long been known that heavy irradiation at levels far above 100 eV/16-amu can produce dark, spectrally neutral residues in carbonaceous materials (e.g., Strazzulla and Johnson, 1991), and Moroz et al. (2003) have now further demonstrated this effect with initially red organics. In Figure 5 we show that these highest irradiation levels are always reached in times $\leq 10^6$ y at small depths $\lesssim 10^{-6}$ cm due to effects of plasma, suprathermal, and lower energy ACR ions which have not been considered in previous models. In the absence of other surface modification processes we might then expect all KBOs to have blackened neutral crusts at these depths. At greater depth the lower dosage rates from more energetic ions could produce organic molecules and reddening from more basic primordial components, but the steep increases in dosage times with depth suggest that these are initially produced in thin layers, particularly at 40 to 85 AU. Within the oldest, dynamically cold KBOs, the reddened layer may extend to meter depths due to secondary interactions, but the outer neutral crust would be correspondingly thicker.

4. Collisional Resurfacing Revisited

A competition between cosmic ray irradiation, presumed to cause reddening due to formation of complex organics, and collisional gardening, bringing more pristine, spectrally neutral ices to the visible surfaces, was first proposed (Luu and Jewitt, 1996) to account for the color diversity of KBOs from a growing number of spectroscopic observations. There has been an ongoing debate about whether there is a bimodal distribution of colors (Tegler and Romanishin, 2000, 2003) or whether the distribution is more continuous (Jewitt and Luu, 2001; Hainaut and Delsanti, 2002) from neutral to very red. Within the classical KBO population there are apparent correlations of more neutral colors with increasing inclination (Trujillo and Brown, 2002) and collision impact speeds (Stern, 1996, 2002), suggestive of collisional resurfacing effects. However, the meaning of these correlations is currently in dispute (Thébault and Doressoundiram, 2003), and the dynamically 'hotter', more neutral objects might have different primordial origins and dynamical ages than the 'colder', redder objects at lower inclination and eccentricity. The same correlations are neither found in the Plutino population of KBOs at the same semimajor axis distance as Pluto, which should be even more collisionally affected than the classical KBOs, nor in the highly eccentric population of Scattered KBOs. Thébault (2003) has helpfully noted at this workshop that the current confusion on the color diversity problem may arise from a present misunderstanding of the basic physical processes involved, including effects of a potentially large population of small Scattered KBOs impacting on the main belt.

We suggest that the additional process missing from previous discussions of the color diversity problem is the slow but steady gardening of Classical KBO surfaces by micrometeoroid impacts from a combination of interstellar grains at high velocity $\sim$26 km/s and KBO dust grains (e.g., Landgraf et al., 2002) at lower velocity. These small impacts are capable of driving global shifts in color by slowly exposing moderately reddened buried material below heavily irradiated crusts of dynamically cold KBOs. Surface modification of dynamically hot KBOs would be driven by larger impactors digging up large volumes of minimally irradiated, more neutral material. A critical role for KBO dust grains, varying (e.g., increasing) in residence time and density with radial position in the Classical Kuiper Belt, might further explain color-orbit correlations in this KBO population. Ultimately this problem may be resolved by New Horizons direct measurements of KBO surface composition and of flux distributions for ions and dust in the KBO region. In the interim, our work continues with available data to model resurfacing.

Added in proof: Finally, Figure 5(A) suggests that the 'cold' KBOs have existed for billions of years in a broad zone near 40 AU of moderate irradiation from galactic cosmic ray ions at micron to meter depths. This region is bounded on the sunward side by increasing fluxes of solar energetic ions and anti-sunward by rising fluxes of energetic ions diffusing inward from the termination shock. Erosion from plasma sputtering and micrometeoroid impacts remove the accumulation of more

neutral radiation products at sub-micron depths and continually exposes redder products in the sensible layer and deeper from galactic cosmic ray interactions. This special location in the heliospheric environment may therefore be optimal for production and survival of sensible red organics in the radiation mantles of these objects.

Acknowledgements

Support is acknowledged by J. F. Cooper for radiation dosage modeling through Raytheon from the following NASA contracts: NAS5-98156 for the Space Science Data Operations Office project at Goddard Space Flight Center, NASW-99029 and NASW-02005 for the Jovian System Data Analysis Program, and NASW-02037 for the Planetary Atmospheres program. Work at MIT was supported under NASA contract 959203 from JPL to MIT and NASA grant NAGS5-11623. C. Wang is also supported in part by NNSFC 40204009 of China. Voyager 1 and 2 position data were provided by the HelioWeb spacecraft ephemeris service of the National Space Science Data Center at http://nssdc.gsfc.nasa.gov/ space/helios/heli.html.

References

Burlaga, L. F., Ness, N. F., Belcher, J. W., Lazarus, A. J., and Richardson, J. D.: 1996, 'Voyager Observations of the Magnetic Field, Interstellar Pickup Ions and Solar Wind in the Distant Heliosphere', *Sp. Sci. Rev.* **78**, 33–42.

Cooper, J. F., Christian, E. R., and Johnson, R. E.: 1998, 'Heliospheric Cosmic Ray Irradiation of Kuiper Belt Comets', *Adv. Sp. Res.* **21**, 1611–1614.

Cooper, J. F., Christian, E. R., and Johnson, R. E.: 2001a, 'Heliospheric Interactions with Kuiper Belt Objects', in *Proc. 27th Intern. Cosmic Ray Conf., Hamburg, August 7–15, 2001*, Vol. 10, pp. 4267–4270.

Cooper, J. F., Johnson, R. E., Mauk, B. H., Garrett, H. B., and Gehrels, N.: 2001b, 'Energetic Ion and Electron Irradiation of the Icy Galilean Satellites', *Icarus* **149**, 133–159.

Cummings, A. C. and Stone, E. C.: 1996, 'Composition of Anomalous Cosmic Rays and Implications for the Heliosphere', *Sp. Sci. Rev.* **78**, 117–128.

Cummings, A. C. and Stone, E. C.: 1998, 'Anomalous Cosmic Rays and Solar Modulation', *Sp. Sci. Rev.* **83**, 51–62.

Doressoundiram, A.: 2003, 'Colour Properties and Trends in Trans-Neptunian Objects' (this volume).

Doressoundiram, A., Peixinho, N., de Bergh, C., Fornasier, S., Thébault, Ph., Barucci, M. A., and Veillet, C.: 2002, 'The Color Distribution in the Edgeworth–Kuiper Belt', *Astron. J.* **124**, 2279–2296.

Draganić, I. G., Ryan, M. P. Jr., and Draganić, Z. D.: 1987, 'Radiation Dosimetry and Chemistry of a Cometary Nucleus', *Adv. Sp. Res.* **7**, (5)13–(5)16.

Frisch, P. C.: 2000, 'The Galactic Environment of the Sun', *Sci. Amer.* **88**, 52–59.

Hainaut, O. R. and Delsanti, A. C.: 2002, 'Colors of Minor Bodies in the Solar System', *Astron. Astrophys.* **389**, 641–664.

Jewitt, D. C. and Luu, J. X.: 2001, 'Colors and Spectra of Kuiper Belt Objects', *Astron. J.* **122**, 2099–2114.

Johnson, R. E.: 1990, Energetic Charged Particle Interactions with Atmospheres and Surfaces, Springer-Verlag, Heidelberg.

Landgraf, M., Liou, J.-C., Zook, H. A., and Grün, E.: 2002, 'Origins of Solar System Dust beyond Jupiter', *Astron. J.* **123**, 2857–2861.

Luu, J. and Jewitt, D.: 1996, 'Color Diversity among the Centaurs and Kuiper Belt Objects', *Astron. J.* **112**, 2310–2318.

Mewaldt, R. A., Liewer, P. C., and the Interstellar Probe Science and Technology Definition Team: 2001a, 'Scientific Payload for an Interstellar Probe Mission', in K. Scherer et al. (eds.), *The Outer Heliosphere: The Next Frontiers, COSPAR Colloquia Series*, Vol. 11, Pergamon, pp. 451–464.

Mewaldt, R. A. et al.: 2001b, 'Long Term Fluences of Energetic Particles in the Heliosphere, in R. F. Wimmer-Schweingruber (ed.), *Solar and Galactic Composition, AIP Conf. Proc. 598*, AIP, Melville, NY, pp. 165–170.

Moore, M. H., Hudson, R. L., and Ferrante, R. F.: 2003, 'Radiation Products in Processed Ices Relevant to Edgeworth–Kuiper-Belt Objects' (this volume).

Moroz, L. V., Baratta, G., Distefano, E., Strazzulla, G., Dotto, E., and Barucci, M. A.: 2003, 'Ion Irradiation of Asphalite: Optical Effects and Implications for Trans-Neptunian Objects and Centaurs' (this volume).

Stern, S. A.: 1996, 'Signatures of Collisions in the Kuiper Disk', *Astron. Astrophys.* **310**, 999–1010.

Stern, S. A.: 2002, 'Evidence for a Collisional Mechanism Affecting Kuiper Belt Object Colors', *Astron. J.* **124**, 2297–2299.

Stern, A. and Spencer, J.: 2003, 'New Horizons: The First Reconnaissance Mission to Bodies in the Kuiper Belt' (this volume).

Stone, E. C.: 2001, 'News from the Edge of Interstellar Space', *Science* **293**, 55–56.

Stone, E. C., Cummings, A. C., and Webber, W. R.: 1996, 'The Distance to the Solar Wind Termination Shock in 1993 and 1994 from Observations of Anomalous Cosmic Rays', *J. Geophys. Res.* **101**, 11017–11026.

Stone, E. C. and Cummings, A. C.: 2001, 'Estimate of the Location of the Solar Wind Termination Shock', in *Proc. 27th Intl. Cosmic Ray Conf., Hamburg*, Vol. 10, pp. 4263–4266.

Strazzulla, G. and Johnson, R. E.: 1991, 'Irradiation Effects on Comets and Cometary Debris', in R. L. Newburn, Jr. et al. (eds.), *Comets in the Post Halley Era*, Vol. I, Kluwer Academic Publishers, Dordrecht, pp. 243–275.

Strazzulla, G., Cooper, J. F., Christian, E. R., and Johnson, R.E.: 2003, 'Ion irradiation of TNOs: From the Fluxes Measured in Space to the Laboratory Experiments', *C.R. Physique*, **4**, 791–801.

Tegler, S. C. and Romanishin, W.: 2000, 'Extremely Red Kuiper-Belt Objects on Near-Circular Orbits Beyond 40 AU', *Nature* **407**, 979–981.

Tegler, S. C. and Romanishin, W.: 2003, 'Resolution of the Kuiper Belt Object Color Controversy: Two Distinct Color Populations', *Icarus* **161**, 181–191.

Thébault, P.: 2003, 'A Numerical Check of the Collisional Resurfacing Scenario', in this proceedings.

Thébault, P. and Doressoundiram, A.: 2003, 'Colors and Collision Rates within the Kuiper Belt: Problems with the Collisional Resurfacing Scenario', *Icarus* **162**, 27–37.

Trujillo, C. A. and Brown, M. E.: 2002, 'A Correlation between Inclination and Color in the Classical Kuiper Belt', *Astrophys. J.* **566**, L125–L128.

Tylka, A. J. et al.: 1997, 'CREME96: A Revision of the Cosmic Ray Effects on Micro-Electronics Code', *IEEE Trans. Nucl. Sci.* **44**, 2150–2160.

Vasyliunas, V. M.: 1971, 'Deep Space Plasma Measurements', in R. H. Lovberg and H. R. Griem (eds.), *Methods of Experimental Physics*, Vol. 9, *Plasma Physics*, Part B, Academic Press, New York, pp. 49–88.

Wang, C. and Richardson, J. D.: 2001, 'Energy Partition between Solar Wind Protons and Pickup Ions in the Distant Heliosphere: A Three-Fluid Approach', *J. Geophys. Res.* **106**, 29401–29408.

Wang, C. and Richardson, J. D.: 2003, 'Determination of the Solar Wind Slowdown near Solar Maximum', *J. Geophys. Res.* **108**(A2), 1058, doi:10.1029/2002JA009322.

Webber, W. R. and Potgieter, M. S.: 1989, 'A New Calculation of the Cosmic-Ray Antiproton Spectrum in the Galaxy and Heliospheric Modulation Effects on This Spectrum Using a Drift Plus Wavy Current Sheet Model', *Astrophys. J.* **344**, 779–785.

Whang, Y. C. and Burlaga, L. F.: 2002, 'Voyager Crossing of the Termination Shock: Prediction', *Adv. Sp. Res.* **29**, 445–450.

Whang, Y. C., Burlaga, L. F., and Ness, N. F.: 1996, 'Pickup Protons in the Heliosphere', *Sp. Sci. Rev.* **78**, 393–398.

Wood, B. E. and Linsky, J. L.: 1997, 'A New Measurement of the Electron Density in the Local Interstellar Medium', *Astrophys. J.* **474**, L39–L42.

Yamamoto, S. and Mukai, T.: 1998, 'Dust Production by Impacts of Interstellar Dust on Edgeworth–Kuiper Belt Objects', *Astron. Astrophys.* **329**, 785–791.

Zank, G. P. and Frisch, P. C.: 1999, 'Consequences of a Change in the Galactic Environment of the Sun', *Astrophys. J.* **518**, 965–973.

Ziegler, J. F., Biersack, J. P., and Littmark, U.: 1985, The Stopping and Range of Ions in Solids, Pergamon Press, New York.